CHEMISTRY
A EUROPEAN JOURNAL

DOI: 10.1002/chem.200903546

Towards Molecular Design Rationalization in Branched Multi-Thiophene Semiconductors: The 2-Thienyl-Persubstituted α-Oligothiophenes

Tiziana Benincori,[b, e] Valentina Bonometti,[c] Filippo De Angelis,[d] Luigi Falciola,[c] Michele Muccini,[f] Patrizia R. Mussini,[c] Tullio Pilati,[e] Giovanni Rampinini,[a] Simona Rizzo,[e] Stefano Toffanin,[f] and Francesco Sannicolò*[a]

Abstract: The introduction of branching in multi-thiophene semiconductors, although granting the required solubility for processing, results in an increased molecular fluxionality and a higher level of distortion, thus hampering π conjugation. Accordingly, branched oligothiophenes require rationalization of their structure–reactivity relationships for target-oriented design and optimization of the synthetic effort. Our current research on spiderlike oligothiophenes affords deep insight into the subject, and introduces new, easily accessible molecules with attractive functional properties. In particular, a regular series, **T′*X*$_Y$**, of five new multi-thiophene systems, **T′5$_3$**, **T′8$_4$**, **T′11$_5$**, **T′14$_6$**, and **T′17$_7$**, constituted by five, eight, 11, 14, and 17 thiophene units, respectively, their longest α-conjugated chain consisting of tri-, tetra-, penta-, hexa-, and heptathiophene moieties, respectively, has been synthesized and fully characterized from the structural, spectroscopic, and electrochemical point of view. The electronic properties of the monomers and their electropolymerization ability are discussed and rationalized as a function of their molecular structure, particularly in comparison with the series of 5-(2,2′-dithiophene)yl-persubstituted α-oligothiophenes (**T*X*$_Y$**) previously reported by us. These oligothiophenes are easily accessible materials, with promising properties for applications as active layers in multifunctional organic devices including solar cells.

Keywords: conducting materials · conjugation · dendrimers · oligothiophenes · structure–activity relationships

Introduction

We have recently reported the results of an investigation on the synthesis and electro-optical properties of 5-(2,2′-dithiophene)yl-persubstituted thiophene (**T9$_5$**), dithiophene (**T14$_6$**), and trithiophene (**T19$_7$**) (spiderlike oligothiophenes) and on the characterization of the materials resulting from their electrochemical oxidation[1] (Scheme 1). The design of these molecules was based on the results of an extensive literature examination demonstrating that, in the case of multi-thiophene molecules, the number of units constituting the longest α-conjugated chain (n_α) is much more important than the overall number of thiophene units constituting the molecule (n) for determining the electronic and optical

[a] Dr. G. Rampinini, Prof. F. Sannicolò
Dipartimento di Chimica Organica e Industriale
and C.I.MA.I.NA. Istituto di Scienze e Tecnologie Molecolari
Università di Milano
via Venezian 21, 20133 Milano (Italy)
Fax: (+39) 02-50314139
E-mail: francesco.sannicolo@unimi.it

[b] Prof. T. Benincori
Dipartimento di Scienze Chimiche ed Ambientali
Università dell'Insubria
via Valleggio 11, 22100 Como (Italy)

[c] Dr. V. Bonometti, Dr. L. Falciola, Prof. P. R. Mussini
Dipartimento di Chimica Fisica ed Elettrochimica
Università di Milano
via Golgi 19, 20133 Milano (Italy)

[d] Dr. F. De Angelis
Istituto di Scienze e Tecnologie Molecolari
Consiglio Nazionale delle Ricerche
via Elce di Sotto 8, 06123 Perugia (Italy)

[e] Prof. T. Benincori, Dr. T. Pilati, Dr. S. Rizzo
Istituto di Scienze e Tecnologie Molecolari
Consiglio Nazionale delle Ricerche
via Golgi 19, 20133 Milano (Italy)

[f] Dr. M. Muccini, Dr. S. Toffanin
Istituto per lo Studio dei Materiali Nanostrutturati
Consiglio Nazionale delle Ricerche
via P. Gobetti 101, 40129 Bologna (Italy)

Supporting information for this article is available on the WWW under http://dx.doi.org/10.1002/chem.200903546.

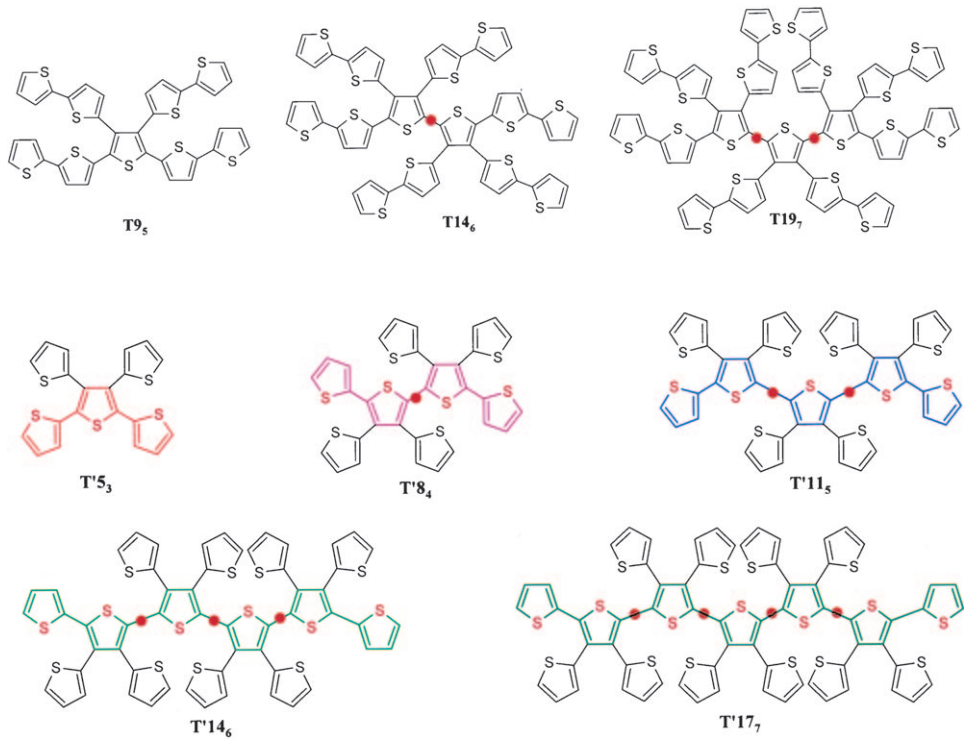

Scheme 1. The $\mathbf{TX_Y}$ series and the new $\mathbf{T'X_Y}$ series. Red circles indicate "nodes" in the main α-conjugated backbone (see text for discussion).

properties of the material, in particular the optical energy gap E_g (calculated from either λ_{max} or λ_{onset}). Even more interesting was the observation that the energy gap value decreases with the increase of the number of α-interconnected thiophene moieties (n_α) with a clear tendency to flatten when five/six conjugated units are present ($n_\alpha \approx 5$–6). In our opinion, the synthetic effort required to prepare molecules constituted by a very large number of thiophene rings is not paralleled by the acquisition of extraordinary conjugation properties, even though other interesting physical features are usually acquired.

The most striking features of **T9$_5$**, **T14$_6$**, and **T19$_7$** and of the corresponding electro-oxidation "polymers" (mainly dimers) are: an outstanding stability towards external agents; their resistance under repetitive electrochemical cycling, even at negative potentials; the similarity of the spectroscopic properties in solution and in the solid state; and their remarkable solubility in organic nonpolar solvents. The introduction of 2-thienyl units on the β positions of an α-oligothiophene backbone produces effects on solubility that are very similar to those generated by conventional alkyl substitution. The thiophene rings connected to the α-conjugated backbone through α–β junctions can also contribute to the spreading and stabilization of the charges injected into the conjugated backbone.[1]

Herein, we report the results of an investigation into the synthesis and the electrochemical and spectroscopic properties of five members of a new series of oligothiophenes, which are structurally related to the above spiderlike systems but are much more easily accessible. These compounds are characterized by an internal core constituted by a single thiophene (**T'5$_3$**), a 2,2′-dithiophene (**T'8$_4$**), a 2,2′,5′,2″-trithiophene (**T'11$_5$**), a 2,2′,5′,2″,5″,2‴-tetrathiophene (**T'14$_6$**), and a 2,2′,5′,2″,5″,2‴,5‴,2⁗-pentathiophene (**T'17$_7$**) moiety, which are fully substituted by 2-thienyl pendant groups (Scheme 1). In the $\mathbf{T'X_Y}$ abbreviations, T means thiophene (the dash indicates that the molecule belongs to the new series), X indicates the total number of thiophene units constituting the molecule (n), and the subscript Y indicates the longest chain displaying α–α′ junctions exclusively (n_α).

The rationale for this design is simple: these molecules appeared as fully characterizable materials, accessible through a few synthetic steps involving inexpensive, commercially available starting materials. In the case of successful experimentation, relevant amounts of these compounds could be prepared through simple scalable procedures. All these oligothiophenes can, in principle, undergo electrochemical polymerization, since all terminal thiophene rings show the preferred polymerization α sites unoccupied.

It is particularly interesting to compare the electronic properties and electropolymerization ability of these conformationally mobile materials with those exhibited by the rather flat and rigid linear α-oligothiophenes $\mathbf{T_N}$ (in which N corresponds to both n and n_α), and by the previously described **T9$_5$**, **T14$_6$**, and **T19$_7$** oligomers, from the perspective of developing reliable rationalization criteria for structure versus reactivity relationships in branched oligothiophenes.

Some preliminary observations on the molecular structure of the $\mathbf{T'X_Y}$ and $\mathbf{TX_Y}$ series can be anticipated at a merely prediction level:

1) In the ground state, significant distortion sites (henceforth called "nodes") can be expected to be localized along the central backbone in the predominant molecular conformation whenever two α-interconnected thiophene rings carry facing thiophene substituents in β positions. Actually, it has already been shown[2] that β substitution induces a distortion from planarity that electronically decouples the resonance extension among different branches, thus introducing a kind of local disorder along the flexible α-conjugated chain, which localizes the π-electron excitations of the thiophene rings.[3]

2) Such nodes are indicated as red circles in Scheme 1, and it is worth noticing that the number of nodes can be rationalized as (n_α−5) in the $\mathbf{TX_Y}$ series and as (n_α−3) in the $\mathbf{T'X_Y}$ series. Therefore, the $\mathbf{TX_Y}$ series has a lower node density per α-linked thiophene unit than the $\mathbf{T'X_Y}$ family.
3) From this perspective, the effective conjugation should be expected to increase with the number of thiophene rings in the main α-linked chain, but be increasingly hampered by an increasing density of nodes along the same backbone. Therefore, a rationalization of the electronic properties in these series (both spectroscopic and electrochemical) should be pivoted on both the n_α value and the node density.

Results and Discussion

Synthesis of $\mathbf{T'5_3}$, $\mathbf{T'8_4}$, $\mathbf{T'11_5}$, $\mathbf{T'14_6}$, and $\mathbf{T'17_7}$: We prepared all the substrates by Stille reaction of the perbromo derivatives of thiophene, 2,2′-dithiophene, 2,2′:5′,2″-trithiophene, 2,2′:5′,2″:5″,2‴-tetrathiophene, and 2,2′:5′,2″:5″,2‴:5‴,2⁗-pentathiophene with commercially available 2-tributylstannylthiophene. All the products, including the unknown dodecabromo-α-tetrathiophene precursor of $\mathbf{T'17_7}$, were fully characterized by analytical and spectral data and, in the case of $\mathbf{T'5_3}$ and $\mathbf{T'8_4}$, by XRD analysis (see below).

$\mathbf{T'5_3}$ (70% yield)[4] and $\mathbf{T'8_4}$ (32% yield) display sharp reversible melting points at 194 and 243 °C (differential scanning calorimetry, DSC), respectively. In the case of $\mathbf{T'11_5}$ (73% yield), $\mathbf{T'14_6}$ (27% yield), and $\mathbf{T'17_7}$ (56% yield), structural assignments and purity controls were based on NMR and mass spectrometry (MS) data.

XRD analysis of $\mathbf{T'5_3}$ and $\mathbf{T'8_4}$: We were able to prepare crystals of $\mathbf{T'5_3}$ suitable for XRD analysis (Figure 1a). It is interesting to compare the $\mathbf{T'5_3}$ structure with that shown by α-trithiophene $\mathbf{T_3}$ in order to forecast its electronic properties: the three α-conjugated rings are quasi-coplanar (torsional angles = 159 and 165°) and not perfectly coplanar as in $\mathbf{T_3}$.[5] Furthermore, some synperiplanar conformers are present that are completely absent in α-trithiophene $\mathbf{T_3}$. Interestingly, the two thiophene rings in the β positions of the central unit are nearly perpendicular to the average plane of the more conjugated sequence (93° and 80°) and can freely assume a syn- or anticlinal conformation. The situation is very similar to that calculated for $\mathbf{T9_5}$ in which the five rings belonging to the α-conjugated main chain lie on the same plane, whereas the two dithiophene pendant groups are orthogonal to the latter.[1]

These observations suggest that the electrochemical oxidative polymerization of $\mathbf{T'5_3}$ can reasonably be regioselective, as previously demonstrated in the case of $\mathbf{T9_5}$, since the electron abstraction involved in the first step of the process is expected to occur at the termini of the α-conjugated system. In the case of $\mathbf{T'8_4}$ we were also able to prepare

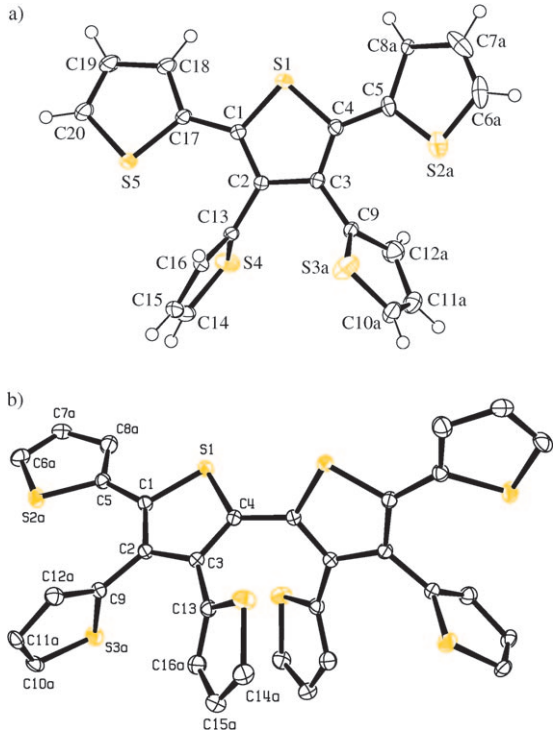

Figure 1. a) ORTEP projection of the preferred conformation of $\mathbf{T'5_3}$ in the S1, S2a, and S5 plane. Disordered atoms are labeled with the letters a and b (b not shown). The a/b population ratio is about 77:23 for the ring connected to C1 and 69:31 for the ring connected to C2. b) ORTEP presentation of $\mathbf{T'8_4}$ (preferred conformation). Only half of the atoms are labeled because there is a twofold symmetry axis nearly perpendicular to the projection plane correlating the two halves. Hydrogen atoms are omitted. Suffix a indicates atomic disorder. *Anti*/*syn* population ratios are: 81:19, 88:12, and 89:11 for the thiophene rings bound to C1, C2, and C3, respectively.

crystals suitable for XRD analysis (Figure 1b). The crystal structure is again very different from that shown by linear α-tetrathiophene $\mathbf{T_4}$, which is a completely flat molecule.[6]

The most consistent sacrifice in conjugation occurs at the level of the two inner rings, which display a remarkable deviation from coplanarity, as already suggested by DFT calculations in the case of $\mathbf{T14_6}$.[1] The torsional angle is about 65°, which corresponds to an unusual synclinal arrangement. The two inner rings are, instead, nearly coplanar with the outer thiophene units (the torsional angle is about 157°). In addition some syn- and antiperiplanar conformations of these rings are observed in the crystal. Similarly to the situation present in the crystal structure of $\mathbf{T'5_3}$, two of the four thiophene rings located in the β position of the central dithiophene system are nearly perpendicular to the plane of the thiophene ring to which they are connected (the torsional angle is about 85°) and can assume either a syn- or antiperiplanar conformation. The torsion between the planes of the two remaining thiophene rings and the plane of the ring to which they are connected is about 43°. Also in this case, oxidative polymerization could in theory be regioselective, involving the α positions of the thiophene rings belonging to the longest conjugated sequence.

Theoretical analysis of T′5$_3$, T′8$_4$, T′11$_5$, and T′14$_6$: To gain insight into the structural, electronic, and optical properties of the investigated systems, we performed DFT and time-dependent DFT (TDDFT) calculations on **T′5$_3$**, **T′8$_4$**, **T′11$_5$**, and **T′14$_6$**, and compared the results with those previously obtained for **T9$_5$** and **T14$_6$**.[1] The ground- and lowest triplet excited-state geometries were optimized without any symmetry constraints by using the PBE0 functional[7,8] and a 6-31g* basis set.[9] On the optimized geometries we calculated several vertical excitations by TDDFT at the same level of theory as that used for geometry optimizations. Although TDDFT calculations at the ground-state geometry correspond to the absorption spectrum, the lowest triplet excited-state geometries are taken here as an approximation to the lowest singlet excited state, the latter corresponding to the emitting state. This approximation allows us to minimize the computational overheads. All the calculations were performed with the Gaussian 03 program package.[10]

The optimized geometry of the singlet ground state (S_0) and lowest triplet excited state (T_1) for **T′5$_3$**, **T′8$_4$**, and **T′11$_5$** are reported in Figure 2. The optimized geometrical conformation of the ground state for **T′8$_4$** is in good agreement with the X-ray structure (see Figure 1); the two central thiophene rings are considerably twisted (SCCS dihedral angle of 58°). All the optimized ground-state structures show a considerable twisting of the thiophene rings: this is particularly evident in the sterically crowded **T′11$_5$** structure, in which the two thiophene units adjacent to the central ring are bound at SCCS dihedral angles close to 60°. Moving to the excited-state structures, the general trend that can be outlined is the planarization of the α-conjugated thiophene backbone relative to the ground state (Figure 2).

As an example, in **T′5$_3$** the SCCS dihedral angle between the central ring and α-bound thiophene units increases from about 151° to 173°, whereas in **T′8$_4$** this parameter reduces from 58° to 23°. A rationale for this behavior can be found by inspecting the frontier molecular orbitals of the investigated species. A schematic representation of the ground-state frontier molecular orbitals at the S_0 and T_1 optimized geometries is reported in Figure 3, along with isodensity plots of such orbitals for **T′5$_3$**.

Qualitatively similar molecular orbitals are calculated at the S_0 and T_1 geometries, although considerable energy shifts are found. A similar electronic structure is calculated for all the investigated species: the HOMO is a π orbital delocalized across the α-fused thiophene system, followed at lower energy by a series of orbitals localized on the β-linked rings. The LUMO is the π* counterpart of the HOMO, and is therefore delocalized across the fused thiophenes, whereas the LUMO+1 is delocalized throughout the entire molecular system. As can be noticed from Figure 3, the HOMO–LUMO gap decreases from 4.01 to 3.81 eV on going from **T′5$_3$** to **T′8$_4$**, whereas negligible differences are calculated between **T′8$_4$** and **T′11$_5$**.

Most notably, dramatic energy differences in the HOMO and LUMO are calculated on going from the S_0 to the T_1 optimized geometries, whereas the other frontier orbitals

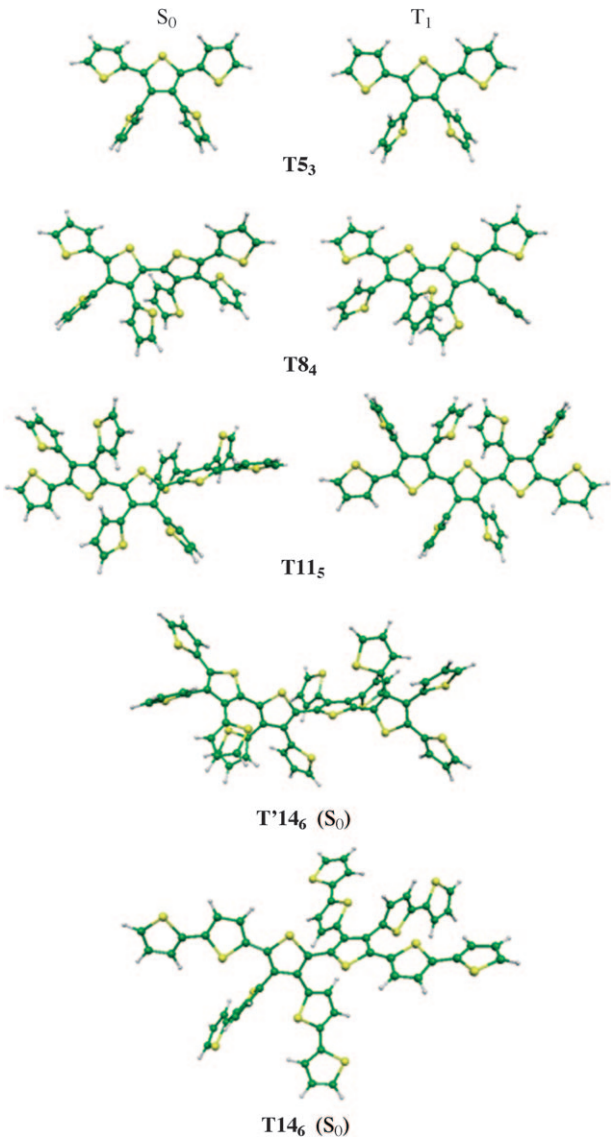

Figure 2. Optimized geometrical structures of the ground state (S_0) and of the lowest excited triplet state (T_1) of **T′5$_3$**, **T′8$_4$**, and **T′11$_5$**, and optimized molecular structures of the ground state of the related **T′14$_6$** and **T14$_6$**.

are much less sensitive to geometrical changes. The HOMO is raised in energy by 0.61, 0.73, and 0.84 eV, whereas the LUMO is stabilized by 0.50, 0.67, and 0.69 eV in **T′5$_3$**, **T′8$_4$**, and **T′11$_5$**, respectively. The HOMO–LUMO gaps are correspondingly reduced in T_1 relative to S_0. These orbital energy differences are clearly related to the planarization of the structures calculated in T_1 relative to S_0. The extent of LUMO stabilization is somehow a measure of the effective conjugation in these systems, which seems therefore to saturate in **T′11$_5$**.

We then performed TDDFT excited-state calculations at both the S_0 and T_1 geometries, thus simulating the absorption and emission processes, respectively. We stress once again that although no approximations are introduced in the calculation of the absorption spectrum at the considered

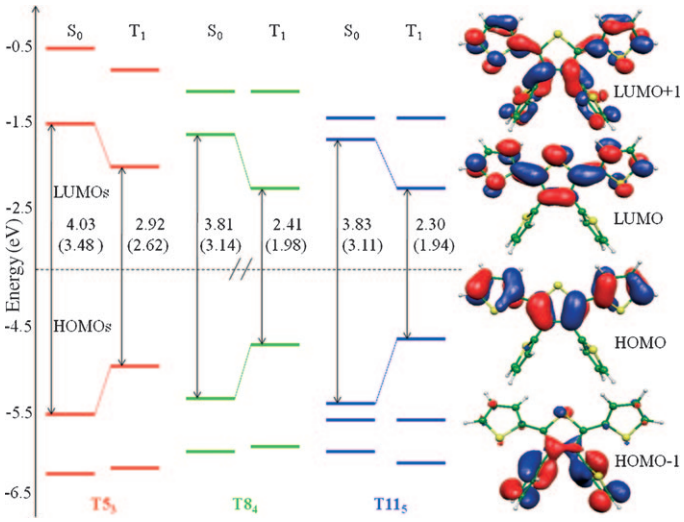

Figure 3. Frontier molecular orbitals for the ground state at the S_0 and T_1 optimized structures of **T′5$_3$**, **T′8$_4$**, and **T′11$_5$**. HOMO–LUMO gaps and lowest excitation energies (data in parentheses) are also reported. Isodensity molecular orbital plots for **T′5$_3$** are displayed on the right-hand side.

level of theory, the use of T_1 rather than S_1 geometries to compute emission transitions represents an approximation, which is checked a posteriori by comparison with experimental data.

The calculated data for **T′5$_3$** are in good agreement with the available experimental results (see below), with maximum deviations of 0.04 and 0.15 eV for absorption and emission data, respectively. The agreement between theory and experiment is slightly less satisfactory for **T′8$_4$** and **T′11$_5$**. Nevertheless, our calculations correctly reproduce the similar optical properties of **T′8$_4$** and **T′11$_5$** and the redshift of the absorption and emission spectra observed on going from **T′5$_3$** to **T′8$_4$** and **T′11$_5$**. The lowest excited states are in all cases originated by single HOMO–LUMO excitations. The redshift observed on going from **T′5$_3$** to **T′8$_4$** and **T′11$_5$** is therefore readily explained in terms of the molecular orbital energy diagram of Figure 3.

We further computationally explored the difference in electronic structure between the related **T14$_6$** and **T′14$_6$** systems, which, despite showing the same values for n and n_α, are found to exhibit rather different electronic properties (see below). The optimized ground-state structures (see Figure 2) immediately show a remarkable difference between the two systems, with **T14$_6$** showing a maximum number of planar conjugated thiophene units equal to three, whereas the number is reduced to two in **T′14$_6$**. This is evident considering the high nonplanarity of the latter structure, which induces a large number of "nodes", thus substantially decreasing the conjugation length. This has important spectroscopic and electrochemical consequences, which can be traced back to the different electronic structure of the two systems. In particular, the LUMO of **T14$_6$** is calculated to lie 0.6 eV below that of **T′14$_6$** due to the increased conjugation in the former, in line with the findings of the electrochemical characterization (see below).

Spectroscopic properties of T′X_Y: A synopsis of the absorption spectra of **T′5$_3$**, **T′8$_4$**, **T′11$_5$**, **T′14$_6$**, and **T′17$_7$**, dissolved in CH_2Cl_2 at the same 10^{-5} M concentration, is reported in Figure 4 and the corresponding key parameters are summarized in Table 1. In all cases, absorption by the main α-conjugated chain is accounted for by the band at wavelengths higher than 330 nm. Its increasing broadness accounts for an increasingly large variety of conformers of different conjugation efficiency as the number of thiophene units increases.

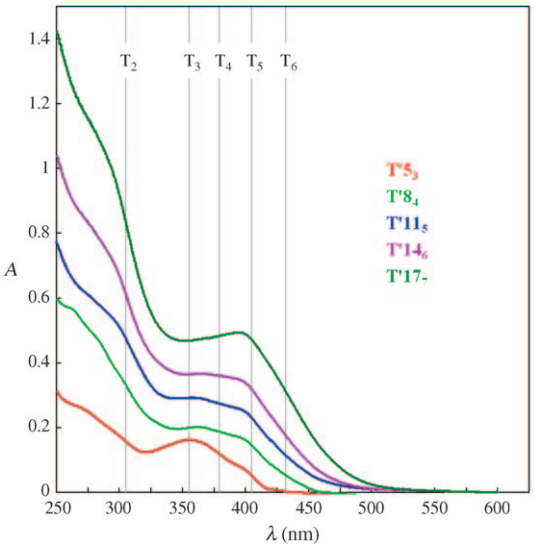

Figure 4. Absorption spectra of the **T′X_Y** compounds in 10^{-5} M CH_2Cl_2 solutions. Vertical bars indicate the literature values of absorption maxima wavelengths for linear oligothiophenes **T$_Y$** consisting of n (n=2–6) α-conjugated thiophene units.[11]

In the case of **T′5$_3$**, such a broad signal shows an absolute maximum at 362 nm, in satisfactory agreement with literature data for α-trithiophene (357 nm, shifting to 370 nm upon alkylation of the thiophene terminals), and a low-energy shoulder at about 392 nm, which is near to the 418 nm maximum expected for a linear quinquethiophene.[12] This spectroscopic fingerprint confirms that the most abun-

Table 1. UV/Vis characterization of **TX_Y** and **T′X_Y** compounds: UV/Vis absorption maxima and onset wavelengths, λ_{max} and λ_{onset}, and the corresponding bandgap energies, $E_{g,max}$ and $E_{g,onset}$.

Compound	λ_{max} [nm]	λ_{onset} [nm]	$E_{g,max}$ [eV[	$E_{g,onset}$ [eV]
T′5$_3$	362	425	3.42	3.92
T′8$_4$	370	460	3.35	2.69
T9$_5$	419	500	2.96	2.48
T′11$_5$	375	490	3.30	2.53
T14$_6$	420	515	2.96	2.41
T′14$_6$	370	500	3.35	2.48
T′17$_7$	400	510	3.10	2.43
T19$_7$	421	523	2.95	2.37

dant **T′5$_3$** conformer presents an effective conjugation length of about three thiophene units with a molecular structure consisting of a nearly planar three-membered α-linked chain with nearly perpendicular β-linked thiophenyl pendant groups.

Differently from the **T′5$_3$** case, absorption peaks for **T′8$_4$**, **T′11$_5$**, **T′14$_6$**, and **T′17$_7$** do not correspond to those of the corresponding linear α-oligothiophenes **T$_4$**, **T$_5$**, **T$_6$**, and **T$_7$**.[11] This finding is consistent with the presence of nodes along the main conjugated backbone: the increasing nonplanarity of the molecule with increasing size induces a hindered delocalization of the excitation over highly distorted conjugated branches. Also, the increase of the full width at half maximum (FWHM) of the peaks with molecular size (FWHM from 66 to 106 nm) corroborates this hypothesis: an increasingly larger distribution of conjugation chain lengths in the molecules accounts for the increasingly broader absorption spectra.

The relatively small redshift of the absorption maxima with increasing molecular dimensions indicates the partially inhibited delocalization of the electronic excitation when the nominal length of the α-conjugated chain is increased, and provides further evidence about the presence of nodes along the chain. Indeed, the presence of chain nodes affects the peak maxima wavelengths more than the onset wavelengths, because the former are related to the most abundant conformation(s) and the latter to the conformations with the highest conjugation efficiency, even if poorly populated (Table 1).

A comparison between **T′14$_6$** and **T14$_6$** (same n and n_α values) may help in highlighting the relationship between molecular structure and electronic properties in the two series, since the absorption spectra of the two molecules are remarkably different (Figure 5). In particular, both the onset and the maximum absorption wavelengths exhibit a significant blueshift when passing from **T14$_6$** to **T′14$_6$**; this nicely accounts for the reduced conjugation in the main, six-membered α-conjugated backbone with increasing node density, that is, (n_α−3) instead of (n_α−5). In the **T′14$_6$** absorption spectrum we observe the disappearance of the high-energy peak (which is related in **T14$_6$** to the decorating dithienyl units β-linked to the central backbone[1]) together with the appearance of a shoulder at about 292 nm, the absorbance of which is nearly proportional to the number of β-linked thiophene pendant groups (see Figure 6). These features confirm that β-linked thiophene or dithiophene units should be regarded as nearly independent, and hardly participating in the lower-energy absorption processes involving the main chain. This scenario supports our attempt to describe the properties of **T′*X*$_Y$** in terms of n_α modulated by the node density.

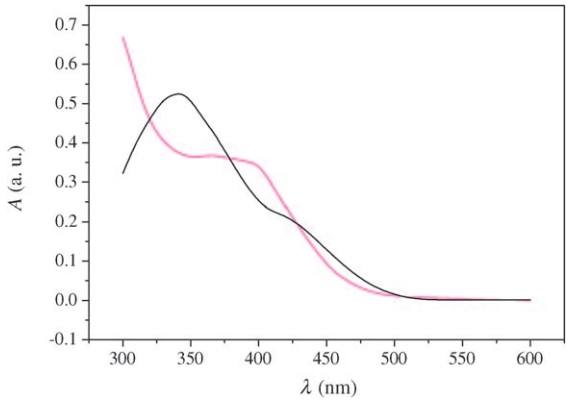

Figure 5. Absorption spectra of 2-thienyl-persubstituted α-sexithiophene (**T′14$_6$**, magenta curve) and 5-(2,2′-dithiophene)yl-persubstituted 2,2′-dithiophene (**T14$_6$**, black curve) in 10^{-5} M CH_2Cl_2 solution.

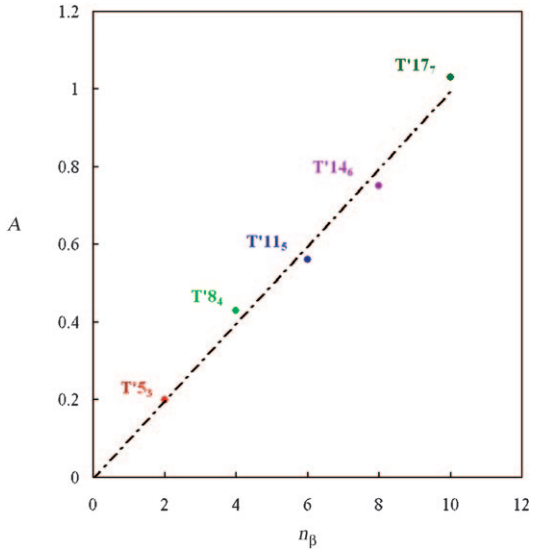

Figure 6. Absorbances of the five **T′*X*$_Y$** molecules at 292 nm plotted as a function of the number of thiophene pendant groups in β positions (n_β) along the main conjugated chain.

Such an approach is satisfactory for determining the onset energy gap ($E_{g,onset}$) values as a function of $1/n$ or $1/n_\alpha$ for the **T′*X*$_Y$** and **T*X*$_Y$** series and the reference model series of linear α-oligothiophenes **T$_N$** (Figure 7 a,b, respectively). The dependence of $E_{g,onset}$ on $1/n$ (Figure 7 a) is described by straight lines for all three oligothiophene series. The straight line generated by the members of the **T′*X*$_Y$** series is placed above that generated by the **T*X*$_Y$** molecules, and both of them are above that of the reference **T$_N$** oligomers. This is perfectly consistent with a regular decrease in conjugation efficiency when the total number of thiophene rings is kept constant.

As already observed in our former study,[1] the plotting of $1/n_\alpha$ affords a sort of normalization (Figure 7 b) and the three series show a similar behavior. Remarkably, the **T′*X*$_Y$** line is again placed above that for **T*X*$_Y$**, but this time both of them are slightly below the reference **T$_N$** line. This could be justified considering that we are looking at the onset values, which do not refer to the most populated conformers but to the most conjugated ones.

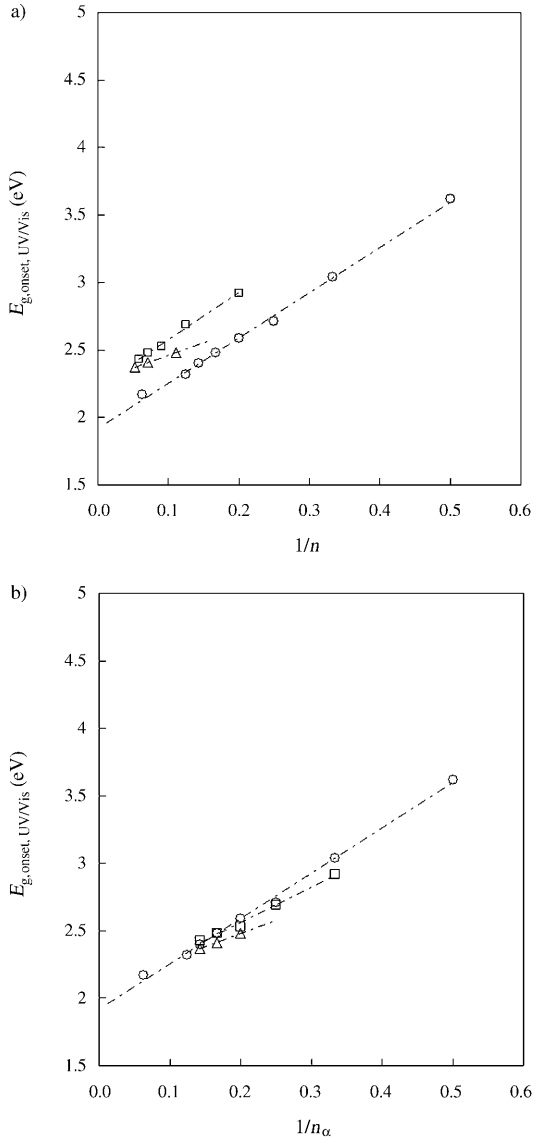

Figure 7. HOMO–LUMO energy gaps (from onset absorption wavelengths) plotted as a function of a) the total thiophene number n, and b) the highest number of α,α′-interconnected thiophenes n_α, for the $\mathbf{T}_N$ linear oligothiophene model series (○), the $\mathbf{TX}_Y$ spiderlike series (△), and the $\mathbf{T'X}_Y$ series (□).

Concerning the optical emission properties, in Figure 8 we report the photoluminescence (PL) spectra of **T′5$_3$**, **T′8$_4$**, **T′11$_5$**, **T′14$_6$**, and **T′17$_7$** molecules dissolved in 10^{-5} M CH_2Cl_2 solution. All the PL spectra are broad and featureless, and each curve can be well interpolated by three Lorentzians. The fact that the PL spectrum of **T$_3$**[11] is structured and redshifted with respect to that of **T′5$_3$** indicates that even for the simplest molecule of the series, the emitting state is only partly related to the longest α-conjugated branch and that the torsional motions of the thiophene moieties broaden the emission spectrum.

As is expected when increasing the nominally longest $1/n_\alpha$ conjugated chain in branched oligothiophenes, the maximum emission wavelength redshifts (from 453 nm for **T′5$_3$** to

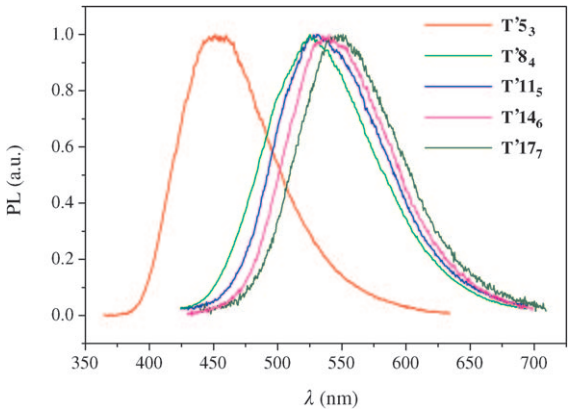

Figure 8. Normalized PL spectra of $\mathbf{T'X}_Y$ in 10^{-5} M CH_2Cl_2 solutions.

548 nm for **T′17$_7$**). The emission spectrum of the $\mathbf{T'X}_Y$ family (**T′5$_3$**) is much more shifted towards the high-energy spectral range with respect to all the other members of the family. As was suggested by the DFT calculations (see above), the **T′5$_3$** ground- and lowest excited-state conformations are very similar, thus resulting in a smaller Stokes shift.[14] For the other members of the series, the conformations corresponding to the ground state and to the lowest-energy excited state are significantly different in terms of planarity.

It is interesting to point out that the emission peak of **T14$_6$**[1] is redshifted by about 31 nm with respect to that shown by **T′14$_6$**. It is likely that the lowest-energy-state conformations in $\mathbf{TX}_Y$ are more conjugated, and so more planar, than the corresponding ones in $\mathbf{T'X}_Y$. Moreover, we can observe that the peripheral rings contribute poorly to the conjugation along the central backbone both in $\mathbf{TX}_Y$ and $\mathbf{T'X}_Y$ oligothiophenes. Upon considering the emission peak FWHM values, they decrease with increasing molecular size (from 98 nm for **T′8$_4$** to 93 nm for **T′17$_7$**) with the exception of **T′5$_3$**. Although at room temperature the FWHM can be taken as a rough measurement of inhomogeneous broadening of the emitting state, intramolecular static disorder seems to be lowered in these molecules due to the structural rigidity of the excited molecule configuration.

In the PL time-resolved measurements reported in Figure 9 we note that the molecules from **T′5$_3$** to **T′14$_6$** present time-decay profiles at the emission maxima that can be well fitted by monoexponential curves. Instead, the **T′17$_7$** temporal decay is well fitted by a biexponential curve with an initial time constant of about 136 ps merging into a tail of 256 ps, with the amplitude of the slower component being the larger one ($A \approx 0.6$).

The regular increase of the lifetime constants with increasing molecular dimensions (Table 2) is a consequence of the increasing stabilization induced by the main α-conjugated chain. Indeed, in the lowest-energy excited state the nodes are not present.

In general, the delocalization of the excitation is expected to hinder the conformational process, thus leading to increased fluorescence decay time.[13] Nevertheless, the fast relaxation of the excited states of all the spiderlike oligothio-

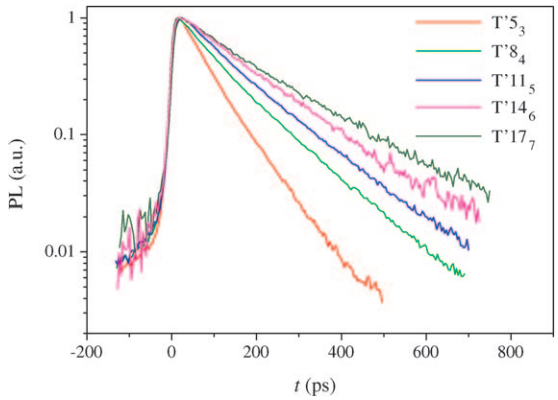

Figure 9. PL time decay t of $\mathbf{T'}\boldsymbol{X_Y}$ in 10^{-5} M CH_2Cl_2 solutions at the emission maxima. The intensity is normalized at $T=0$.

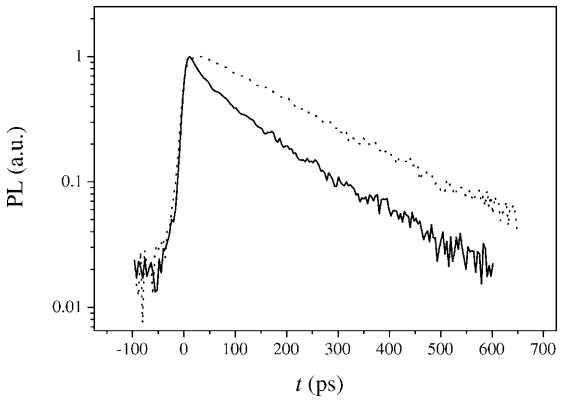

Figure 10. PL time decay of $\mathbf{T'17_7}$ in 10^{-5} M CH_2Cl_2 solutions in the emission spectral ranges 500–510 nm (donor rise curve, ——) and 590–600 nm (acceptor decay curve, •••••). PL intensity is normalized at $T=0$.

Table 2. Lifetime constants [ps] of $\mathbf{T'}\boldsymbol{X_Y}$ in 10^{-5} M CH_2Cl_2 solutions at the maximum emission wavelength.

$\mathbf{T'5_3}$	$\mathbf{T'8_4}$	$\mathbf{T'11_5}$	$\mathbf{T'14_6}$	$\mathbf{T'17_7}$
73	110	130	160	256 136

phenes in solution can be ascribed to the large number of nonradiative pathways promoted by the complex architecture of these macromolecules, which may intervene to dissipate the excitation energy.

Indeed, a nonradiative intramolecular energy-transfer process is particularly evident in the largest molecule of the $\mathbf{T'}\boldsymbol{X_Y}$ family, $\mathbf{T'17_7}$, the exciton dynamic of which is more appropriately described by a distribution of lifetimes, thus revealing that a more complex process, apart from a vibrational relaxation, is taking place. We also mention that the $\mathbf{T'14_6}$ exciton dynamics in the very early times after excitation shows the typical features of an energy transfer (see the Supporting Information). In the case of $\mathbf{T'17_7}$, the lifetime constant values (146 and 27 ps) of the high-energy portion of the emission spectrum (solid decay curve in Figure 10) are smaller than those at the maximum emission wavelength. The low-energy PL decay profile (dotted decay curve in Figure 10) can be described by a monoexponential curve with a 200 ps single-lifetime constant. Moreover, at early times there is an initial buildup in PL intensity that reaches a maximum value after 7 ps, whereupon the signal starts its natural decay.

We suggest that a Coulombic process of excitation energy transfer from longer to shorter conjugated chains takes place within the complex architecture of the molecule after excitation. In particular, Coulombic theory, in its simplest form such as Förster theory, can describe the $\mathbf{T'17_7}$ radiative relaxation because the high-energy PL decay can be well fitted by the Förster decay function.[14,15]

Clearly, in spiderlike oligothiophenes we cannot simply identify the donor as the periphery moieties and the acceptor as the core locus as reported in many dendrimeric systems,[16] because $\mathbf{T'}\boldsymbol{X_Y}$ and $\mathbf{T}\boldsymbol{X_Y}$ are all-thiophene molecules and the energy hierarchy is related only to the lengths of the α-conjugated chains. Moreover, as the absorption and steady-state emission properties highlighted, the complex conformation of these sterically hindered macromolecules prevents us obtaining a straightforward determination of the extension of the α-conjugated branches. Nevertheless, it can be considered that the energy migration occurs by an excitonic-type coherent transport mechanism, and not by incoherent hopping among thiophene branches, since we observe a time-dependent reduction of the FWHM of the spectrum.

Electrochemical properties of $\mathbf{T'}\boldsymbol{X_Y}$: The electrochemical activity of $\mathbf{T'}\boldsymbol{X_Y}$ oligomers was investigated by cyclic voltammetry (CV) in 5×10^{-4} M CH_2Cl_2 solutions, with tetrabutylammonium perchlorate (TBAP; 0.1 M) as supporting electrolyte, on glassy carbon (GC) electrodes. The results are summarized in Table 3, which presents CV data of onset and peak potentials for the first oxidation and reduction process, together with the relevant energy gaps, to be compared with the absorption data reported in Table 1.

Peak potentials and energy gaps: Both Table 3 and Figure 12 show the first oxidation peak potentials, $E_{p,a}$, only slightly shifting to less positive values with increasing n_α, and remaining nearly constant for the three larger $\mathbf{T'}\boldsymbol{X_Y}$ compounds. Such $E_{p,a}$ values afford an approximate estimation of the HOMO energy levels for the five molecules (also reported in Table 3) by use of Equation (1):[17,18]

$$E_{HOMO}\ [eV] \approx -1e(E_{p,a}\ [V\ vs.\ Fc^+|Fc] + 4.8\ [V\ Fc^+|Fc\ vs.\ zero]) \quad (1)$$

ultimately based on the absolute value for the normal hydrogen electrode (NHE) critically assessed in a fundamental review paper.[19]

More significant, albeit moderate, appears the positive shift of the first reduction peak potentials, $E_{p,c}$, with increasing n_α. They in turn afford an approximate estimation of the

Table 3. Voltammetric characterization of $\mathbf{TX_Y}$ and $\mathbf{T'X_Y}$ monomers. Upper section: first oxidation and reduction peak potentials $E_{p,a}$ and $E_{p,c}$, recorded at scan rate $v = 0.2\ V\,s^{-1}$, with derived HOMO and LUMO energy levels, $E_{H[max]}$ and $E_{L[max]}$ and bandgap energies $E_{g,max\,EC}$. Lower section: first oxidation and reduction onset potentials $E_{onset,a}$ and $E_{onset,c}$, recorded at scan rate $v = 0.2\ V\,s^{-1}$, with derived HOMO and LUMO energy levels, $E_{H[onset]}$ and $E_{L[onset]}$, and bandgap energies $E_{g,onset\,EC}$. All potentials are referred to the $Fc^+|Fc$ standard redox couple.

	$E_{p,a}$ [V (Fc^+|Fc)]	$E_{p,c}$ [V (Fc^+|Fc)]	$E_{H[max]}$ [eV]	$E_{L[max]}$ [eV]	$E_{g,max\,EC}$ [eV]	$E_{onset,a}$ [V (Fc^+|Fc)]	$E_{onset,c}$ [V (Fc^+|Fc)]	$E_{H[onset]}$ [eV]	$E_{L[onset]}$ [eV]	$E_{g,onset\,EC}$ [eV]
$\mathbf{T'5_3}$	0.711	−2.653	−5.51	−2.15	3.36	0.605	−2.405	−5.41	−2.40	3.01
$\mathbf{T'8_4}$	0.632	−2.465	−5.43	−2.34	3.10	0.515	−2.365	−5.32	−2.44	2.88
$\mathbf{T9_5}$	0.518	−2.199	−5.32	−2.60	2.72	0.405	−1.915	−5.21	−2.89	2.32
$\mathbf{T'11_5}$	0.612	−2.495	−5.41	−2.31	3.11	0.515	−2.275	−5.32	−2.53	2.79
$\mathbf{T14_6}$	0.582	−2.155	−5.38	−2.65	2.74	0.455	−1.985	−5.26	−2.82	2.44
$\mathbf{T'14_6}$	0.614	−2.465	−5.41	−2.34	3.08	0.475	−2.295	−5.28	−2.51	2.77
$\mathbf{T'17_7}$	0.612	−2.385	−5.41	−2.42	3.00	0.505	−2.225	−5.31	−2.58	2.73
$\mathbf{T19_7}$	0.552	−2.275	−5.35	−2.53	2.83	0.435	–	−5.24	–	–

LUMO energy levels for the five molecules (also reported in Table 3) by use of Equation (2):

$$E_{LUMO}\ [eV] \approx -1e(E_{p,c}\ [V\ vs.\ Fc^+|Fc] + 4.8\ [V\ Fc^+|Fc\ vs.\ zero]) \quad (2)$$

In this homogeneous series of oligothiophenes the inductive effects can be assumed to be fairly constant, and therefore the small variations in $E_{p,a}$ and $E_{p,c}$ should merely reflect a limited increase of the effective conjugation length with increasing thiophene number, which of course results in a limited increase of the π-system ability to stabilize both the radical cation (formed at $E_{p,a}$) and radical anion (formed at $E_{p,c}$).

Such polaron stabilization ability is accounted for in a more straightforward way by the distance between $E_{p,a}$ and $E_{p,c}$, thus affording calculation of the electrochemical HOMO–LUMO energy gap [Eq. (3)]:

$$\begin{aligned} E_{g,EC}\ [eV] &= -(E_{HOMO}\ [eV] - E_{LUMO}\ [eV]) \\ &= 1e(E_{p,a}\ [V\ vs.\ Fc^+|Fc] - E_{p,c}\ [V\ vs.\ Fc^+|Fc]) \end{aligned} \quad (3)$$

In the present homogeneous series of oligothiophenes inductive effects due to polar substituents are absent, and thus it could be reasonably assumed that the redox site would be the same for radical cation and radical anion formation. Therefore the energy gap should neatly account for the conjugation efficiency of the π system.

Such electrochemical HOMO–LUMO energy gaps, calculated both from peak maxima and from peak onsets, as in the case of UV–visible gaps, are reported in Table 3. Although electrochemical and spectroscopic energy gaps do not coincide, they appear to be in a fairly linear relationship (Figure S2 in the Supporting Information).

It is worthwhile remarking that such a difference between optical and electrochemical data is often observed and quite reasonable, since optical data concern electron promotion between intramolecular levels, whereas the electrochemical information accounts for electron transfer between molecule and electrode with concurrent formation of net positive or negative charges. Accordingly, the solvent and supporting electrolyte effects can also be significantly different in the two cases.

First oxidation peak morphology and polymerization ability of $\mathbf{T'X_Y}$: Like in the former $\mathbf{TX_Y}$ series,[1] in the new $\mathbf{T'X_Y}$ family the polymerization ability also regularly decreases with increasing molecular complexity, as is evident from the comparison of subsequent oxidative cycles (Figure 11). In particular:

1) $\mathbf{T'5_3}$ features a chemically irreversible first oxidation peak accounting for a fast irreversible chemical reaction following the first electron transfer, and an irregular return peak typically accounting for the formation of an electrochemically active layer on the electrode surface; consistently, it undergoes fast and regular polymerization. The oligomerization rate increases with increasing concentration, as expected considering the radical cation coupling mechanism usually assumed for thiophene polymerization.[20]
2) The $\mathbf{T'8_4}$ peak, albeit similar to the previous one, shows some trace of chemical reversibility; consistently, the polymerization rate is lower (and, again, it increases with increasing substrate concentration).
3) The case of $\mathbf{T'11_5}$ could be considered borderline: at the lower concentration tested (0.0005 M) it features two nearly coincident, chemically reversible monoelectronic peaks and, consistently, no polymerization is observed; however, increasing the concentration results in the formation of a small amount of conducting polymer.
4) The cases of $\mathbf{T'14_6}$ and $\mathbf{T'17_7}$ feature a single peak that, according to its height (relative to the former cases and also considering that the diffusion coefficients in the systematic $\mathbf{T'X_Y}$ series must regularly decrease with increasing bulkiness), should correspond to the extraction of two electrons from two equivalent and completely independent redox sites.

One possible explanation for the gradual decrease in the $\mathbf{T'X_Y}$ polymerization ability with increasing n could be found, in principle, in the increased solubility resulting from

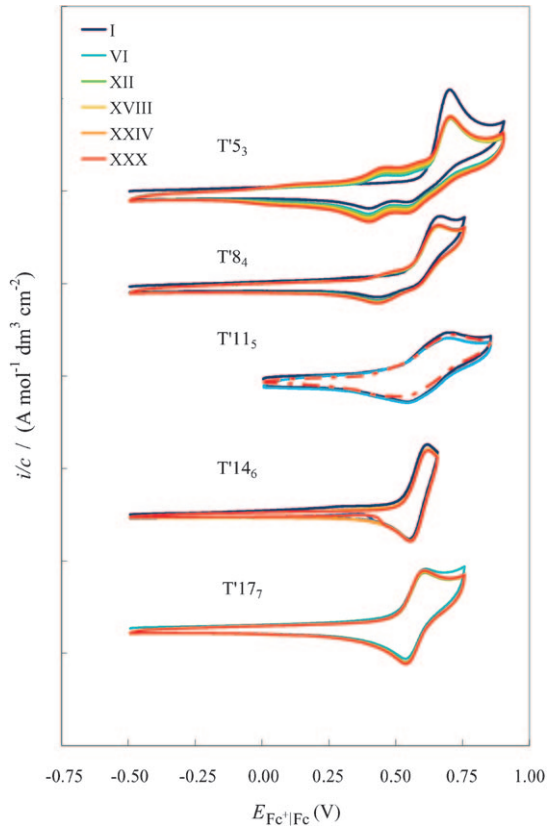

Figure 11. Synopsis of the oxidation region of the CV characteristics of the five $\mathbf{T'}\boldsymbol{X}_{\boldsymbol{Y}}$ oligomers (recorded on a GC electrode in CH_2Cl_2 solution, in the presence of 0.1 M TBAP, at 0.2 V s^{-1} potential scan rate), which contrasts the first cycle (blue curve) and selected subsequent cycles.

increasing molecular branching, as observed, for example, in a recent study concerning thiahelicenes;[21] however, in the present case this explanation would not justify the reversible peak shape. In other words, in the case of formation of a soluble coupling product the irregular return peak corresponding to the redox-active film could disappear, but the oxidation peak would maintain an irreversible shape. On the other hand, simply justifying the increasing peak reversibility and decreasing polymerization ability in terms of increasing length of the conjugated system also appears to be unsatisfactory because, as we have said before, the effective conjugation is nearly constant after the first term (as indicated by both spectroscopic and electrochemical HOMO and LUMO data). A more convincing explanation could be found in the increasing difficulty for two radical cations (possibly localized on the two α positions of the terminal thiophene rings in the main conjugated chain) to come across in the favorable position for coupling with increasing molecular bulkiness.

The shape of the peak morphology for the last three compounds of the $\mathbf{T'}\boldsymbol{X}_{\boldsymbol{Y}}$ series can be explained by considering the node localization in each molecule (red circles in Scheme 1):

1) The three molecules have the same terminals, which consist of a tetrathiophene unit including two α-linked thiophene rings. The charge should be localized on these terminals, which can be considered two equivalent redox centers, connected by a π system partially impaired by nodes, at increasing distance from each other.
2) Under such conditions, it is reasonable that in $\mathbf{T'11_5}$ the two identical homotopic terminal systems, separated by a single thiophene unit, could weakly interact, thus giving rise to two subsequent peaks (tending to merge, but still distinguishable) because the energy required to extract an electron from the second terminal is slightly higher (since it perceives the positive charge formed on the first terminal). Instead, in the larger molecules, the distance from the termini and the number of nodes in between mean that the two redox sites are totally independent (with an exception made for a small entropy term related to the probability of subsequently involving two sites located in the same molecule)[22] and a single peak of width 57 mV is found, as in the case of a simple monoelectronic reversible electron transfer (albeit the height is doubled).

The polymers obtained from the first three molecules of the series are stable upon repeated potential cycling around the first oxidation peak in a monomer-free solution.

The onset energy gaps in the polymer films (Figure 12) are smaller than in the starting oligomers, thus pointing to an enhanced conjugation. As has already been mentioned, we observed that after five or six thiophene units in the main chain no significant improvement is obtained in these compounds; therefore, the narrower gap could be at least partially justified in terms of π-stacking interactions in the

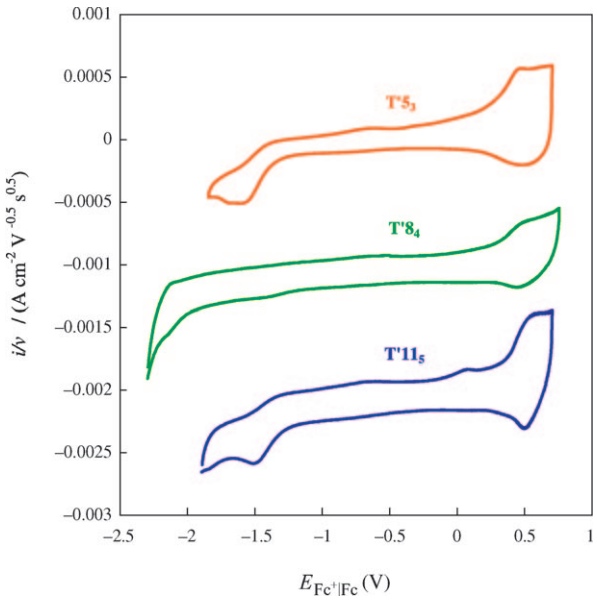

Figure 12. Synopsis of charge-trapping effects in the polymer films deposited from the first three compounds in the $\mathbf{T'}\boldsymbol{X}_{\boldsymbol{Y}}$ series on a GC electrode in CH_2Cl_2 in the presence of 0.1 M TBAP (stationary cycles).

solid-state film. Figure 12 also shows that, unlike the $\mathbf{TX_Y}$ series, only slight traces of the charge-trapping effects can be perceived in the new polymer series.

Conclusion

A five-term series of easily accessible multi-thiophene molecules $\mathbf{T'X_Y}$ has been prepared and fully characterized from the analytical and structural point of view. The electrochemical and optical properties of these compounds have been carefully investigated and compared with the results obtained in the case of the $\mathbf{TX_Y}$ series (spiderlike oligothiophenes) previously studied by us, assuming as a reference the $\mathbf{T_N}$ family of α-conjugated linear oligothiophenes. By taking advantage of the conspicuous number of compounds now available, some interesting structure–property relationships have been deduced, which will be very helpful in designing new materials for optoelectronics and photonics.

As for the physical properties, the main advantages acquired by the multi-thiophene substitution of the $\mathbf{T_N}$ backbone, both with 2-thienyl and 2-(5,2′-dithienyl) groups, are the good solubility of these materials in organic aprotic solvents and their outstanding stability under electrochemical cycling, in particular that of the electropolymerization products even in the oxidized state.

The electronic properties are nearly exclusively dependent upon:

1) The number of thiophene units constituting the longest α-conjugated chain (n_α), independently of the overall number of thiophene rings constituting the molecule (n).
2) The number of nodes distributed along this chain ($n-5$ for the $\mathbf{TX_Y}$ and $n-3$ for the $\mathbf{T'X_Y}$ series). Upon increasing the node number, a regular decrease in the efficiency of conjugation is observed as a consequence of the progressive distortion of the main α-conjugated backbone from planarity. This could imply that the effective conjugation level exhibited by the completely flat family of α-oligothiophenes could not be attained by any branched, more or less distorted members of the $\mathbf{TX_Y}$ and $\mathbf{T'X_Y}$ series.

Support for this observation is supplied by the higher α,α-conjugation level present in the $\mathbf{TX_Y}$ with respect to the $\mathbf{T'X_Y}$ series, as expected when considering the node density in systems belonging to the two series displaying identical n and n_α values. Indeed, a striking demonstration is given by the $\mathbf{T'14_6}$ (three nodes) and $\mathbf{T14_6}$ (one node) couple, for which the former shows a more positive electrochemical oxidation peak potential [0.61 vs. 0.58 V ($Fc^+|Fc$)], more negative reduction peak potential [−2.47 vs. −2.16 V ($Fc^+|Fc$)], blueshifted absorption maximum (420 vs. 370 nm), and higher electrochemical (3.08 vs. 2.74 eV) and optical (3.35 vs. 2.96 eV) energy gap. These differences are strongly reduced when the onset values of both electrochemical and UV data are compared. The use of the onset values is acceptable in multifunctional systems in which many components contribute to the electronic excitation processes. Thus, the onset values of the absorption wavelengths for $\mathbf{T'14_6}$ and $\mathbf{T14_6}$ are 500 and 515 nm with a calculated gap of 2.48 and 2.41 eV, respectively. Also, the oxidative potential onsets are very similar for the two compounds [0.48 vs. 0.46 V ($Fc^+|Fc$)], with consequent rather similar calculated energy gaps (2.77 vs. 2.44 eV).

If this procedure is adopted for all the members of the three series, very nice linear relationships are found, which demonstrate that the electronic properties of dendrimeric all-thiophene oligomers are very similar to those exhibited by the parent $\mathbf{T_N}$ family, independently of the total number of thiophene units present in the molecule.

Also, in the $\mathbf{T'X_Y}$ series some flattening of the onset energy gap values is observed when the main α-conjugated chain reaches five or six units. On the contrary, as expected, the absorbance progressively increases in both the $\mathbf{TX_Y}$ and $\mathbf{T'X_Y}$ series when the total number of thiophene units n increases. This is a further demonstration that hyperbranched molecules are not required for reducing the energy gap in thiophene oligomers, whereas a great number of thiophene moieties is important if high extinction coefficients are required, as in materials designed for solar-cell devices.

Experimental Section

Organic synthesis: NMR spectra were obtained on Bruker AV 400, Bruker AC 300, and Avance 500 spectrometers. Chemical shifts were recorded in ppm and the coupling constants were reported in Hertz. Mass spectra were recorded on a VG AUTOSPEC M246 spectrometer. DSC curves were recorded on a Mettler DSC 823 apparatus. THF was freshly distilled from sodium/benzophenone. All reagents were commercially available and were used as received. The normal workup included extraction, drying over Na_2SO_4, and evaporation of volatile materials in vacuo. Purifications by column chromatography were performed with Merck silica (70–230 mesh).

Tetrakis[3′,4′,3″,4″-(thiophen-2-yl)]-2,2′:5′,2″:5″,2‴-tetrathiophene ($\mathbf{T'8_4}$): 2-Tributylstannylthiophene (10.8 g, 28.9 mmol) and $[Pd(PPh_3)_4]$ (0.80 g, 0.69 mmol) were added under a nitrogen atmosphere to a stirred solution of hexabromo-2,2′-dithiophene (3.0 g, 4.73 mmol) in toluene (150 mL). The mixture was heated under reflux for 18 h and filtered on a short silica-gel column to remove the catalyst residue. Toluene was evaporated under reduced pressure and the residue was purified by chromatography (silica gel, hexane/chloroform 7:3) to give $\mathbf{T'8_4}$ as a yellow-orange solid (1.0 g, 32%). M.p. (DSC) 243 °C; ^{1}H NMR (300 MHz, $CDCl_3$): $\delta = 7.39$ (dd, $^3J(H,H) = 5.1$, $^4J(H,H) = 1.2$ Hz, 2H), 7.24 (dd, $^3J(H,H) = 5.1$, $^4J(H,H) = 1.2$ Hz, 2H), 7.21 (dd, $^3J(H,H) = 5.1$, $^4J(H,H) = 1.2$ Hz, 2H), 7.07 (dd, $^3J(H,H) = 3.7$, $^4J(H,H) = 1.2$ Hz, 2H), 7.04 (dd, $^3J(H,H) = 4.1$, $^3J(H,H) = 5.1$ Hz, 2H), 6.93 (m, 4H), 6.88 (dd, $^3J(H,H) = 3.6$, $^3J(H,H) = 5.1$ Hz, 2H), 6.75 ppm (dd, $^3J(H,H) = 3.6$, $^4J(H,H) = 1.2$ Hz, 2H); ^{13}C NMR (400 MHz, $CDCl_3$): $\delta = 137.11$ (C), 136.58 (C), 136.13 (C), 135.99 (C), 135.73 (C), 131.06 (C), 130.26 (CH), 130.14 (C), 128.95 (CH), 127.82 (CH), 127.40 (CH), 127.23 (CH), 126.97 (CH), 126.81 ppm (CH); MS (EI): m/z: 658 [M^+]; HRMS: m/z: calcd for $C_{32}H_{18}S_8^+$: 657.917425; found: 657.916500; elemental analysis calcd (%) for $C_{32}H_{18}S_8$: C 58.32, H 2.75, S 38.92; found: C 58.03, H 2.55, S 38.62.

Hexakis[3′,4′,3″,4″,3‴,4‴-(thiophen-2-yl)]-2,2′:5′,2″:5″,2‴:5‴,2⁗:5⁗,2′′′′-tetrathiothiophene ($\mathbf{T'11_5}$): 2-Tributylstannylthiophene (635 mg, 1.7 mmol) and $[Pd(PPh_3)_4]$ (40 mg, 0.039 mmol) were added under a nitrogen atmosphere to a stirred solution of octabromo-α-trithiophene (3 g, 4.73 mmol)

in xylene (15 mL). The mixture was heated under reflux for 20 h, then filtered on a short silica-gel column to remove the catalyst residue. The solvent was evaporated under reduced pressure and the residue was purified by chromatography (silica gel, hexane/chloroform 7:3) to yield **T′11$_5$** as a brown-orange solid (113 mg, 73%). M.p. = 232 °C; ^{1}H NMR (400 MHz, $CDCl_3$): δ = 7.36 (dd, ^3J(H,H) = 5.2, ^4J(H,H) = 1.1 Hz, 2H), 7.25 (dd, ^3J(H,H) = 5.1, ^4J(H,H) = 1.1 Hz, 2H), 7.21 (dd, , ^3J(H,H) = 5.1, ^4J(H,H) = 1.1 Hz, 2H), 7.18 (dd, ^3J(H,H) = 5.1, ^4J(H,H) = 1.2 Hz, 2H), 7.02 (dd, ^3J(H,H) = 3.7, ^4J(H,H) = 1.2 Hz, 2H), 7.01 (dd, ^3J(H,H) = 5.1, ^3J(H,H) = 3.6 Hz, 2H), 6.92 (dd, ^3J(H,H) = 3.6, ^4J(H,H) = 0.97 Hz, 2H), 6.9 (m, 4H), 6.84 (dd, ^3J(H,H) = 5.1, ^3J(H,H) = 3.6, Hz, 2H,), 6.72 (dd, ^3J(H,H) = 3.6, ^4J(H,H) = 1.1 Hz, 2H), 6.66 ppm (dd, ^3J(H,H) = 3.6, ^4J (H,H) = 1.1 Hz, 2H); ^{13}C NMR (400 MHz, $CDCl_3$): δ = 137.09 (C), 136.74 (C), 136.09 (C), 135.93 (C), 135.89 (C), 135.68 (C), 135.08 (C), 133.79 (C), 130.91 (C), 130.23 (CH), 129.85 (C), 129.34 (CH), 128.95 (CH), 127.77 (CH), 127.36 (CH), 127.19 (CH), 127.14 (CH), 127.04 (CH), 126.94 (CH), 126.86 (CH), 126.78 ppm (CH); MS (EI): *m/z*: 904 [M^+]; HRMS: *m/z*: calcd for $C_{44}H_{24}S_{11}^+$: 903.880591; found: 903.886170; elemental analysis calcd (%) for $C_{44}H_{24}S_{11}$: C 58.37, H 2.67, S 38.96; found: C 58.06, H 2.57, S 38.67.

Octakis[3′,4′,3″,4″,3‴,4‴,3⁗,4⁗-(thiophen-2-yl)]-2,2′:5′,2″:5″,2‴:5‴,2⁗:5⁗,2⁗′:2⁗′,5⁗′-sexithiophene (T′14$_6$): 2-Tributylstannylthiophene (1.97 g, 4.8 mmol) and [Pd(PPh$_3$)$_4$] (0.28 g, 0.24 mmol) were added under a nitrogen atmosphere to a stirred solution of decabromo-α-tetrathiophene (0.54 g, 0.48 mmol)[23] in xylene (15 mL). The mixture was heated under reflux for 48 h and filtered on a short silica-gel column to remove the catalyst residue. Xylene was evaporated under reduced pressure and the residue was purified by flash chromatography (silica gel, hexane/dichloromethane 1:1) to yield **T′14$_6$** as a yellow solid (0.15 g, 27%). M.p. = 307 °C; ^{1}H NMR (500 MHz, $CDCl_3$): δ = 7.36 (dd, ^3J(H,H) = 5.1, ^4J(H,H) = 1.1 Hz, 2H), 7.24 (dd, ^3J(H,H) = 5.1, ^4J(H,H) = 1.1 Hz, 4H), 7.21 (dd, ^3J(H,H) = 5.1, ^4J(H,H) = 1.1 Hz, 2H), 7.18 (dd, ^3J(H,H) = 5.1, ^4J(H,H) = 1.2 Hz, 2H), 7.01 (m, 4H), 6.92 (m, 4H), 6.88 (m, 4H), 6.85 (dd, ^3J(H,H) = 5.1, ^3J(H,H) = 3.6 Hz, 2H), 6.70 (dd, ^3J(H,H) = 3.5, ^4J(H,H) = 1.2 Hz, 2H), 6.66 (dd, ^3J(H,H) = 3.6, ^4J(H,H) = 1.1 Hz, 2H), 6.64 ppm (dd, ^3J(H,H) = 3.5, ^4J(H,H) = 1.2 Hz, 2H); ^{13}C NMR (500 MHz, $CDCl_3$): δ = 136.72 (C), 136.30 (C), 135.69 (C), 135.54 (C), 135.44 (C), 135.43 (C), 135.28 (C), 134.87 (C), 134.52 (C), 133.37 (C), 133.10 (C), 130.49 (C), 129.84 (CH), 129.41 (C), 128.95 (CH), 128.93 (CH), 128.54 (CH), 127.38 (CH), 126.96 (CH), 126.94 (CH), 126.89 (CH), 126.79 (CH), 126.72 (CH), 126.62 (CH), 126.56 (CH), 126.54 (CH), 126.45 (CH), 126.38 ppm (CH); MS (EI): *m/z*: 1150 [M^+]; HRMS: *m/z*: calcd for $C_{56}H_{30}S_{14}^+$: 1149.843758; elemental analysis calcd (%) for $C_{56}H_{30}S_{14}$: C 58.40, H 2.63, S 38.97; found: C 58.14, H 2.56, S 38.76.

Dodecabromo-α-quinquethiophene: Bromine (12 mL, 237 mmol) was added to a suspension of quinquethiophene (300 mg, 0.73 mmol) in acetic acid (30 mL) and the mixture was heated at 60 °C for 3 days. The solution was treated with a saturated solution of $NaHSO_3$ to remove excess bromine, and the red solid precipitate was collected by filtration (960 mg, 97%). M.p. 320 °C; MS (EI): *m/z*: 1359 [M^+]; HRMS: *m/z*: calcd for $C_{20}Br_{12}S_5^+$: 1346.880392.

Decakis[3′,4′,3″,4″,3‴,4‴,3⁗,4⁗-(thiophen-2-yl)]-2,2′:5′,2″:5″,2‴:5‴,2⁗:5⁗,2⁗′:2⁗′,5⁗′:2‴′,5‴′-sexithiophene (T′17$_7$): 2-Tributylstannylthiophene (2.25 g, 6.25 mmol) and [Pd(PPh$_3$)$_4$] (40 mg, 0.035 mmol) were added under a nitrogen atmosphere to a stirred solution of dodecabromo-α-quinquethiophene (250 mg, 0.26 mmol) in xylene (30 mL). The mixture was heated under reflux for 30 h and filtered on a short silica-gel column to remove the catalyst residue. Xylene was evaporated under reduced pressure to give an oil which, when treated with hexane, gave **T′17$_7$** as an orange solid (200 mg, 56%). M.p. 215 °C; ^{1}H NMR (500 MHz, $CDCl_3$): δ = 7.35 (broad d, ^3J(H,H) = 5.1 Hz, 2H), 7.22 (m, 8H), 7.17 (broad d, *J* = 5.1 Hz, 2H), 7.01 (m, 4H), 6.91 (m, 4H), 6.86 (m, 8H), 6.69 (m, 2H), 6.64 (m, 4H), 6.61 ppm (m, 2H); ^{13}C NMR (500 MHz, $CDCl_3$): δ = 136.70 (C), 136.29 (C), 135.68 (C), 135.52 (C), 135.44 (C), 135.41 (C), 135.38 (C), 135.27 (C), 134.82 (C), 134.80 (C), 134.71 (C), 134.66 (C), 134.48 (C), 133.41 (C), 133.38 (C), 133.09 (C), 133.05 (C), 130.49 (C), 129.84 (CH), 129.42 (C) 128.94 (CH), 128.92 (CH), 128.54 (CH), 127.38 (CH), 126.96 (CH), 126.89 (CH), 126.87 (CH), 126.85 (CH), 126.79 (CH), 126.73 (CH), 126.63 (CH), 126.54 (CH), 126.52 (CH), 126.45 (CH), 126.38 ppm (CH); MS (EI): *m/z*: 1397 [M^+] HRMS: *m/z*: calcd for $C_{68}H_{36}S_{17}^+$: 1395.806924; elemental analysis calcd (%) for $C_{68}H_{36}S_{17}$: C 58.42, H 2.60, S 38.99; found: C 58.24, H 2.46, S 38.54.

Spectroscopy: For spectroscopic measurements the **T′*X*$_Y$** molecules were dissolved in dichloromethane at a concentration of 10^{-5} M. UV–visible absorption spectra were recorded with a JASCO V-550 spectrophotometer. PL was excited with a Ti:sapphire (Spectra Physics) femtosecond laser (pulse duration 100 fs and repetition rate 80 MHz), pumped at 532 nm by a solid-state 10 W continuous-wave laser. The fundamental emission of the Ti:sapphire laser was coupled into a β-barium borate (BBO) crystal for second harmonic generation before exciting the sample PL at a wavelength of 400 nm. PL spectra were then measured by using a Chromex monochromator with a spectral resolution of 2 meV.

Electrochemistry: The monomers were characterized by CV at potential scan rates typically ranging from 0.02 to 2.00 V s^{-1}, by using 0.25–5.00 mM CH_2Cl_2 solutions, deaerated by N_2 purging, with 0.1 M TBAP as the supporting electrolyte. The ohmic potential drop was compensated by the positive feedback technique. The experiments were carried out with an AUTOLAB PGSTAT potentiostat (EcoChemie, Utrecht, The Netherlands) run by a PC with the GPES 4.9 software of the same manufacturer. The working electrode was either i) a GC disk embedded in Teflon (Amel, 0.071 cm^2), ii) a gold disk embedded in Teflon (Amel, 0.0314 cm^2), iii) a platinum foil (1.44 cm^2) for bulk depositions, or iv) an indium-doped tin oxide (ITO)-coated glass slide (Aldrich, sheet resistance 9–12 Ω sq^{-1}). The counter electrode was a platinum wire. The operating reference electrode was either an Ag|AgCl pseudoreference electrode or an aqueous saturated calomel electrode (SCE) with a redox potential of −0.495 V in the CH_2Cl_2 working solution versus that of the Fc^+|Fc couple (the intersolvental redox potential reference currently recommended by the IUPAC)[23] and +0.052 V versus that of the $Me_{10}Fc^+$|$Me_{10}Fc$ couple (an improved intersolvental reference under investigation).[24,25] The optimized polishing procedure for the working disk electrodes consisted of surface treatment with a diamond powder 1 mm in diameter (Aldrich) on a DP-Nap wet cloth (Struers).

Electrochemical oligomerization of the working solution by repeated CV cycling in the potential range of the first anodic peak (or anodic peak system) at a potential scan rate of 0.20 V s^{-1} resulted in deposition of conducting films on the working electrodes. The CV stability of the films was tested by repeated cycling in the same potential range at different scan rates, in monomer-free CH_2Cl_2 solution with 0.1 M TBAP as supporting electrolyte. Finally, the potential range was progressively extended negatively in search of the first reduction potential and possible related charge-trapping phenomena.

Crystallographic data: CCDC-759573 (**T′5$_3$**) and 759572 (**T′8$_4$**) contain the supplementary crystallographic data for this paper. These data can be obtained free of charge from the Cambridge Crystallographic Data Centre via www.ccdc.cam.ac.uk/data_request/cif.

Acknowledgements

This work was supported by MIUR: FIRB-RBNE033KMA "Composti molecolari e materiali ibridi nanostrutturati con proprietà ottiche risonanti e non risonanti per dispositivi fotonici", by the EU Commission: FP7/2007-2013 (PHOTO-FET), and by Fondazione Cariplo "Progettazione e utilizzo di nuovi materiali organometallici o di coordinazione per celle solari organiche di terza generazione". T.B. thanks the Dipartimento di Chimica Organica e Industriale dell'Università degli Studi di Milano for hospitality. The authors are grateful to Dr. Marcello Capaccio for preliminary synthetic work.

[1] T. Benincori, M. Capaccio, F. De Angelis, L. Falciola, M. Muccini, P. Mussini, A. Ponti, S. Toffanin, P. Traldi, F. Sannicolò, *Chem. Eur. J.* **2008**, *14*, 459–471.

[2] C. Xia, X. Fan, J. Locklin, R. C. Advincula, A. Gies, W. Nonidez, *J. Am. Chem. Soc.* **2004**, *126*, 8735–8743.
[3] M. Klessinger, *Excited States and Photochemistry of Organic Molecules*, VCH, Weinheim, **1993**.
[4] a) J. Nakayama, R. Yomoda, M. Hoshino, *Heterocycles* **1987**, *26*, 2215–2222; b) J. Nakayama, K. Sawada, A. Ishii, M. Hoshino, *Heterocycles* **1992**, *34*, 1487–1490; c) S. J. Roberts-Bleming, G. L. Davies, M. Kalaji, P. J. Murphy, A. M. Celli, D. Donati, F. Ponticelli, *J. Org. Chem.* **2003**, *68*, 7115–7118.
[5] F. Van Bolhuis, H. Wynberg, E. E. Havinga, E. V. Meijer, E. G. J. Starling, *Synth. Met.* **1989**, *30*, 381–389; R. Azumi, M. Goto, K. Honda, M. Matzumoto, *Bull. Acad. Vet. Fr.* **2003**, *76*, 1561–1567.
[6] L. Antolini, G. Horowitz, F. Kouki, F. Garnier, *Adv. Mater.* **1998**, *10*, 382–385; T. Siegrist, C. Kloc, R. A. Laudese, *Adv. Mater.* **1998**, *10*, 379–382.
[7] J. P. Perdew, K. Burke, M. Ernzerhof, *Phys. Rev. Lett.* **1996**, *77*, 3865–3868.
[8] C. Adamo, G. E. Scuseria, V. Barone, *J. Chem. Phys.* **1999**, *111*, 2889–2900.
[9] J. S. Binkley, J. A. Pople, W. J. Hehre, *J. Am. Chem. Soc.* **1980**, *102*, 939–947.
[10] Gaussian 03, Revision D01, M. J. Frisch, G. W. Trucks, H. B. Schlegel, G. E. Scuseria, M. A. Robb, J. R. Cheeseman, J. A. Montgomery, Jr., T. Vreven, K. N. Kudin, J. C. Burant, J. M. Millam, S. S. Iyengar, J. Tomasi, V. Barone, B. Mennucci, M. Cossi, G. Scalmani, N. Rega, G. A. Petersson, H. Nakatsuji, M. Hada, M. Ehara, K. Toyota, R. Fukuda, J. Hasegawa, M. Ishida, T. Nakajima, Y. Honda, O. Kitao, H. Nakai, M. Klene, X. Li, J. E. Knox, H. P. Hratchian, J. B. Cross, C. Adamo, J. Jaramillo, R. Gomperts, R. E. Stratmann, O. Yazyev, A. J. Austin, R. Cammi, C. Pomelli, J. W. Ochterski, P. Y. Ayala, K. Morokuma, G. A. Voth, P. Salvador, J. J. Dannenberg, V. G. Zakrzewski, S. Dapprich, A. D. Daniels, M. C. Strain, O. Farkas, D. K. Malick, A. D. Rabuck, K. Raghavachari, J. B. Foresman, J. V. Ortiz, Q. Cui, A. G. Baboul, S. Clifford, Gaussian, Inc., Pittsburgh PA, **2003**.
[11] K. Meerholz, J. Heize, *Electrochim. Acta* **1996**, *41*, 1839–1854.
[12] A. Facchetti, M.-H. Yoon, C. L. Stern, G. R. Hutchinson, M. A. Ratner, T. Marks, *J. Am. Chem. Soc.* **2004**, *126*, 13480–13501.
[13] G. Bongiovanni, C. Botta, G. Di Silvestro, M. A. Loi, A. Mura, R. Tubino, *Chem. Phys. Lett.* **2001**, *345*, 386–394.
[14] M. Pope, C. E. Swenberg, *Electronic Processes in Organic Semiconductors*, Oxford University Press, New York, **1982**.
[15] T. Förster, *Modern Quantum Chemistry, Part 2: Action of Light and Organic Molecules*, Academic Press, New York, **1982**.
[16] O. Varnavski, I. D. W. Samuel, L.-O. Pålsson, R. Beavington, P. L. Burn, T. Goodson III, *J. Chem. Phys.* **2002**, *116*, 8893–8904.
[17] W.-Y. Wong, X.-Z. Wang, Z. He, A. B. Djurisic, C.-T. Yip, K.-Y. Cheung, H. Wang, C. S. K. Mak, W.-K. Chan, *Nat. Mater.* **2007**, *6*, 521–527.
[18] R. S. Ashraf, M. Shahid, E. Klemm, M. Al-Ibrahim, S. Sensfuss, *Macromol. Rapid Commun.* **2006**, *27*, 1454–1459.
[19] S. Trasatti, *Pure Appl. Chem.* **1986**, *58*, 955–966.
[20] G. G. Wallace, G. M. Spinks, L. A. P. Kane-Maguire, P. R. Teasdale, *Conductive Electroactive Polymers*, Taylor & Francis, Boca Raton, **2003**.
[21] A. Bossi, L. Falciola, C. Graiff, S. Maiorana, C. Rigamonti, A. Tiripicchio, E. Licandro, P. R. Mussini, *Electrochim. Acta* **2009**, *54*, 5083–5097.
[22] A. J. Bard, L. R. Faulkner, *Electrochemical Methods*, Wiley-VCH, Weinheim, **2002**, pp. 243–247.
[23] W. Steinkopf, R. Leitsmann, K. H. Hofmann, *Liebigs Ann.* **1941**, *546*, 180–199.
[24] a) G. Gritzner, J. Kuta, *Pure Appl. Chem.* **1984**, *56*, 461–466; b) G. Gritzner, *Pure Appl. Chem.* **1990**, *62*, 1839–1858.
[25] a) L. Falciola, A. Gennaro, A. A. Isse, P. R. Mussini, M. Rossi, *J. Electroanal. Chem.* **2006**, *593*, 47–56; b) J. Ruiz, D. Astruc, *C. R. Acad. Sci. Série IIc* **1998**, *1*, 21; c) I. Noviandri, K. N. Brown, D. S. Fleming, P. T. Gulyas, P. A. Lay, A. F. Masters, L. Phillips, *J. Phys. Chem. A* **1999**, *103*, 6713.

Received: December 24, 2009
Revised: May 4, 2010
Published online: June 25, 2010

